

FLASH MIXING ON THE WHITE DWARF COOLING CURVE: SPECTROSCOPIC CONFIRMATION IN NGC 2808¹

THOMAS M. BROWN², THIERRY LANZ^{3,4}, ALLEN V. SWEIGART⁵, MISTY CRACRAFT², IVAN HUBENY⁶, AND WAYNE B. LANDSMAN⁷

To appear in The Astrophysical Journal

ABSTRACT

We present new *HST* far-UV spectroscopy of two dozen hot evolved stars in NGC 2808, a massive globular cluster with a large population of “blue-hook” (BHk) stars. The BHk stars are found in ultraviolet color-magnitude diagrams of the most massive globular clusters, where they fall at luminosities immediately below the hot end of the horizontal branch (HB), in a region of the HR diagram unexplained by canonical stellar evolution theory. Using new theoretical evolutionary and atmospheric models, we have shown that these sub-luminous HB stars are very likely the progeny of stars that undergo extensive internal mixing during a late He-core flash on the white dwarf cooling curve. This flash mixing leads to hotter temperatures and an enormous enhancement of the surface He and C abundances; these hotter temperatures, together with the decrease in H opacity shortward of the Lyman limit, make the BHk stars brighter in the extreme UV while appearing sub-luminous in the UV and optical. Our far-UV spectroscopy demonstrates that, relative to normal HB stars at the same color, the BHk stars of NGC 2808 are hotter and greatly enhanced in He and C, thus providing unambiguous evidence of flash mixing in the sub-luminous population. Although the C abundance in the BHk stars is orders of magnitude larger than that in the normal HB stars, the atmospheric C abundance in both the BHk and normal HB stars appears to be affected by gravitational settling. The abundance variations seen in Si and the Fe-peak elements also indicate that atmospheric diffusion is at play in our sample, with all of our hot subdwarfs at 25,000 K to 50,000 K exhibiting large enhancements of the iron-peak elements. The hottest subdwarfs in our BHk sample may be pulsators, given that they fall in the temperature range of newly-discovered pulsating subdwarfs in ω Cen. In addition to the normal hot HB and BHk stars, we also obtain spectra of five blue HB stars, a post-HB star, and three unclassified stars with unusually blue UV colors.

Subject headings: globular clusters: individual (NGC 2808) – stars: atmospheres – stars: evolution – stars: horizontal branch – ultraviolet: stars

1. INTRODUCTION

For decades, globular clusters have served as the fundamental laboratory for the study of stellar evolution. Their utility arose from the assumption that, within observational errors, each globular cluster appeared to be comprised of stars with a single age and chemical composition. The subsequent discovery that some globular clusters host multiple stellar generations is one of the most exciting developments in the study of resolved stellar populations. These multiple generations were revealed in the color-magnitude diagrams (CMDs) of the most massive globular clusters; examples include the double main sequence (MS) in ω Cen (Anderson 1997) and the triple MS in NGC 2808 (D’Antona et al. 2005; Piotto et al. 2007). The splitting of the MS in these clusters is thought to be due to the presence of subpopulations having He abundances as high as $Y \sim 0.4$ (Piotto et al. 2005), with these He-rich stars being born from the He-rich ejecta of the initial stellar generation.

The existence of these He-rich subpopulations offers the opportunity to test theories of stellar evolution in a new regime, both in the early evolution on the MS and in the late stages beyond. For example, the CMDs of massive clusters exhibit unusual characteristics on the horizontal branch (HB). Regardless of metallicity, massive clusters tend to host significant populations of extreme HB (EHB) stars at $T_{\text{eff}} > 20,000$ K. These EHB stars have extremely thin envelopes ($\sim 10^{-3}$ to $10^{-2} M_{\odot}$) – the result of extensive mass loss on the red-giant branch (RGB). The analogs of the EHB stars in the field are the subdwarf B (sdB) stars, which produce the “UV upturn” in the otherwise cool spectra of elliptical galaxies (Brown et al. 1997; Brown et al. 2008). In general, the HB of a high-metallicity cluster will be dominated by red clump stars, while the HB of a low-metallicity cluster will extend to hotter stars, although other parameters (such as age, He abundance, and cluster central density) can play a role in determining the HB morphology (e.g., Gratton et al. 2010; Dotter et al. 2010; Fusi Pecci & Bellazzini 1997). At a fixed cluster age, the MS turnoff mass decreases strongly with increasing He abundance, leading to a bluer HB morphology for a given range of RGB mass loss (D’Antona et al. 2002). Because massive clusters are more likely to retain the He-rich ejecta from the initial burst of star formation, He enrichment may explain the presence of hot HB stars in those massive clusters that are metal-rich. For example, in NGC 6388 and NGC 6441, the HB extends to hot temperatures, and slopes upward in optical CMDs from the red clump to the top of the blue HB tail (Rich et al. 1997; Busso et al. 2007), as one would expect if these clusters contained a He-rich subpopulation. The blue HB morphology of NGC 2808 can be similarly explained by

¹ Based on observations made with the NASA/ESA *Hubble Space Telescope*, obtained at STScI, which is operated by AURA, Inc., under NASA contract NAS 5-26555.

² Space Telescope Science Institute, 3700 San Martin Drive, Baltimore, MD 21218; tbrown@stsci.edu, cracraft@stsci.edu

³ Department of Astronomy, University of Maryland, College Park, MD 20742

⁴ Laboratoire Lagrange, UMR7293, Université de Nice Sophia-Antipolis, CNRS, Observatoire de la Côte d’Azur, F-06304 Nice, France; thierry.lanz@oca.eu

⁵ Code 667, NASA Goddard Space Flight Center, Greenbelt, MD 20771; allen.v.sweigart@nasa.gov

⁶ Steward Observatory, University of Arizona, Tucson, AZ 85712; hubeny@aegis.as.arizona.edu

⁷ Adnet Systems, NASA Goddard Space Flight Center, Greenbelt, MD 20771; wayne.b.landsman@nasa.gov

an increasing He abundance (from $0.24 < Y < 0.4$) at increasing temperature (Dalessandro et al. 2011). In this scenario, the EHB stars would be the progeny of the most He-rich MS stars.

Another curiosity in massive clusters is the luminosity dispersion of their EHB stars. In seven massive globular clusters hosting EHB stars, ultraviolet photometry shows that the EHB terminates in a “blue hook” (BHK) of subluminous stars lying up to ~ 1 mag below the canonical HB (D’Cruz et al. 2000; Brown et al. 2001; Brown et al. 2010). As discussed by Brown et al. (2001), the most likely explanation for these stars is a delayed He-core flash. If the RGB mass loss is large enough, a star can evolve off the RGB and undergo a delayed He-core flash either as it crosses the HR diagram (known as an “early hot flasher”) or as it descends the white dwarf cooling curve (known as a “late hot flasher”; Castellani & Castellani 1993; D’Cruz et al. 1996). Note that this evolutionary path does *not* assume the star evolves in isolation; although this evolutionary path is frequently described as “single star evolution” in the literature, it is in fact driven solely by mass loss, whether it occurs in a single star (e.g., stellar winds) or in a binary system (e.g., Roche-lobe overflow and mass transfer). Normally the flash convection does not penetrate into the envelope, due to the high entropy barrier of the strong H-burning shell. However, such penetration is inevitable if He ignites on the white dwarf cooling curve, where the H-burning shell is much weaker. Sweigart (1997) first demonstrated that a flash on the white dwarf cooling curve will mix the H-rich envelope into the stellar interior, thereby greatly enhancing the surface He, C and possibly N abundances. This result was subsequently confirmed by detailed calculations of the flash-mixing phase by Cassisi et al. (2003) and Miller Bertolami et al. (2008). Brown et al. (2010) demonstrated that flash mixing is the only known mechanism that can plausibly produce the low luminosities of the BHK stars in massive clusters. An independent analysis of optical and UV photometry in NGC 2808 reaffirmed this conclusion (Dalessandro et al. 2011). The low ultraviolet and optical luminosities of the flash-mixed stars are primarily due to their higher effective temperatures (which increases the bolometric correction) and the reduction in their H opacity below the Lyman limit (which increases the flux emitted in the extreme ultraviolet at the expense of the flux at longer wavelengths).

A key prediction of the flash mixing scenario is a substantial increase in the surface He and C abundances of the BHK stars. Spectroscopic evidence in support of this prediction has already been found in another massive cluster, ω Cen, by Moehler et al. (2011). They obtained optical spectroscopy of potential BHK stars by selecting targets from the faint end of the hot HB tail in an optical CMD of the cluster. They found that all of the HB stars cooler than 30,000 K were He-poor, while nearly three-fourths of the hotter stars had solar to super-solar He abundances, as well as C abundances up to $\sim 3\%$ by mass. Moreover, these C abundances were strongly correlated with the He abundance.

The He-sdB and He-sdO stars are the most likely field analogs of the BHK stars found in globular clusters. Various formation scenarios have been debated in the literature for this field population, including both flash mixing and white dwarf mergers (see, e.g., Ahmad & Jeffery 2003; Lanz et al. 2004; Stroerer et al. 2007; Heber & Hirsch 2010). Lanz et al. (2004) obtained far-UV spectroscopy of three He-sdB stars, and demonstrated that the incredibly strong C lines in two of them (PG1544+488 and JL87) implied an atmospheric

composition of 1–2% C by mass; they argued that this provided strong evidence of flash mixing in the field population. Ahmad et al. (2004) subsequently found that PG1544+488 (the archetype of the He-sdB class) is a spectroscopic binary of two He-sdB stars; under the invalid assumption that flash mixing is a “single star” evolutionary channel, they argued that binary He-sdB stars present a problem for the flash mixing scenario. However, as we noted above, flash mixing is in fact a natural outcome of extreme mass loss, and does not depend upon how this mass loss occurs. Stroerer et al. (2007) noted that the He-sdO stars occupy a narrow temperature range of 40,000 to 50,000 K, and can be significantly enhanced in C and/or N. Heber & Hirsch (2010) subsequently concluded that the flash-mixing channel is favored over the merger channel in the production of those He-sdO stars that are C-rich. However, the ongoing debate regarding the origin of the He-sdO and He-sdB stars is largely due to the uncertain placement of these stars in the HR diagram relative to the canonical EHB – specifically, it hinges upon the accurate measurement of surface gravity and luminosity (cf. Ahmad & Jeffery 2003; Lanz et al. 2004). Of course, interpretation of an HR diagram constructed from the field population is hampered by uncertainties in distance, reddening, age, and original MS chemical composition. In contrast, these uncertainties are largely avoided in a globular cluster population. Because the BHK populations in the massive globular clusters observed by Brown et al. (2010) are confined to luminosities immediately below the hot end of the zero-age HB, it seems clear that white dwarf mergers cannot play a role in the formation of these stars. If mergers were important, one would expect to find BHK stars with larger masses and therefore brighter luminosities than the luminosity of the canonical EHB. No such stars are observed. Most likely, the field population of He-sdB and He-sdO stars arises from a greater diversity of evolutionary channels, including possibly mergers, than is the case in the globular clusters.

Here, we present recent UV spectroscopy of both normal and subluminous EHB stars in NGC 2808, where the classification comes from high-precision UV photometry. Our objective is to test the flash-mixing scenario by determining the He and C abundances in the BHK stars relative to the abundances in the normal EHB stars; unfortunately, no significant N diagnostics are available in our spectra. In total, spectra were obtained for seven normal EHB stars and eight BHK stars. The sample of subluminous stars includes two stars that have luminosities consistent with other BHK stars but colors significantly redder than the rest of the BHK population, and indeed far redder than expected from flash mixing. We also obtained spectra of five blue HB (BHB) stars, and three unclassified objects with unusually blue UV colors. Finally, our spectroscopy includes a bright post-HB star too hot to ascend the asymptotic giant branch (AGB); such stars are usually classified as AGB-Manqué (AGBM) stars.

2. OBSERVATIONS AND DATA REDUCTION

We obtained spatially-resolved spectra along three slit positions in the center of NGC 2808 using the Space Telescope Imaging Spectrograph (STIS) on the *Hubble Space Telescope* (HST). The program was originally awarded time in 2004, but was withdrawn before any observations were obtained due to the failure of a STIS power supply later that year. The program was re-proposed and re-awarded time in 2008, but due to scheduling constraints, the observations were delayed until September 2010 (one slit position) and February 2011 (two

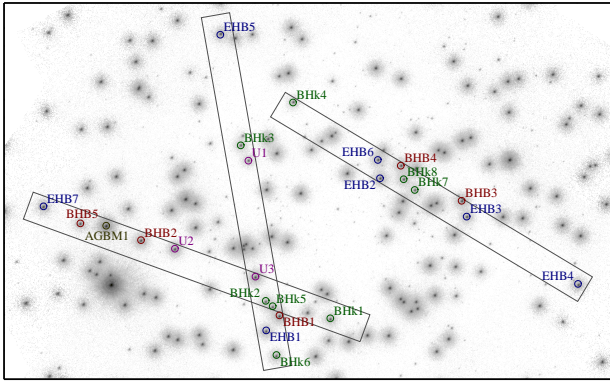


Figure 1. A far-UV image of NGC 2808 (Brown et al. 2001), shown at a logarithmic stretch, with the three spectroscopic slit positions indicated (boxes). Although the slit has dimensions of $52'' \times 2''$, the far-UV detector is only $25''$ across, so we show the slit as truncated by the detector. The sources with clean spectroscopy are labeled according to their evolutionary stage: extreme horizontal branch (EHB), blue hook (BHK), blue horizontal branch (BHB), AGB-Manqué (AGBM), and unclassified (U). The positions of these stars in the UV CMD of NGC 2808 are shown in Figure 2.

additional slit positions). The spectra were obtained with the G140L grating, which provides a resolution of $\sim 300 \text{ km s}^{-1}$, although the spectral purity was degraded slightly by our use of the wide $52 \times 2''$ slit. We chose this wide slit in order to maximize the number of hot stars that could be placed within the slit for a given pointing. The NGC 2808 core is far less crowded in the far-UV than in the optical, and so we were able to obtain clean spectra of 24 hot stars using just three slit positions (Figure 1). These sources sample various evolutionary stages in the UV CMD of NGC 2808 (Figure 2).

Each of the three slit positions was observed for 5 orbits, with two exposures per orbit, giving a total exposure time ranging from 14442 sec to 14460 sec per slit position and a signal-to-noise ratio (SNR) of ~ 20 per resolution element. The resolution and SNR were intended to discriminate between stars that have and have not undergone flash mixing, given the enormous differences in atmospheric abundances between these two possibilities; i.e., the spectra are insufficient to obtain high-precision abundance estimates. For a given slit position, the individual exposures were dithered by a few pixels along the slit, in order to mitigate detector artifacts and flat-field variations. Because we obtained spectra of multiple stars per slit position, our targets are generally offset from the slit midline in the dispersion direction. To correctly align in wavelength the sensitivity curve and the counts spectrum of each star, we measured the position within the slit for each star, both in the dispersion and cross-dispersion directions. This alignment was an iterative process. Our initial position estimates used brief (2 sec) CCD images of the cluster obtained through the $52'' \times 2''$ slit at the start of each observing visit, in conjunction with the far-UV and near-UV images of Brown et al. (2001). We then extracted the spectra using the IRAF X1D package, measured the wavelengths of strong interstellar lines, and tweaked the position of each star in the dispersion direction.

By default, the X1D package estimates the gross source counts from an extraction box centered on the object in question, and subtracts a background estimated from two neighboring extraction boxes. To reduce the noise in this background estimate, the background is smoothed before subtraction. Specifically, X1D replaces the background counts spectrum with a low-order polynomial fit to the background, except for two wavelength regions centered on the bright geo-

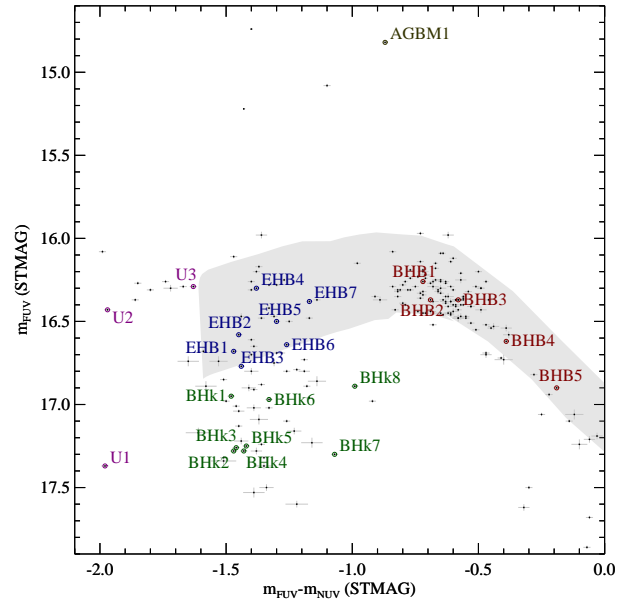


Figure 2. The UV CMD of NGC 2808 (Brown et al. 2001) with labels for those sources with clean far-UV spectroscopy (see Figure 1). The cluster was imaged with the FUV/F25QTZ and NUV/F25CN270 bandpasses on STIS (see Figure 2 of Brown et al. 2001). The photometric errors are indicated (grey crosses). The statistical uncertainty in photometric color is $< 0.02 \text{ mag}$ for our entire spectroscopic sample, and the agreement between the observed and theoretical BHB locus indicates that systematic errors (e.g., instrument calibration, assumed reddening) cannot be large. The canonical HB locus is shaded grey.

coronal lines of Lyman- α $\lambda 1215$ and O I $\lambda 1301$, where the background spectrum changes too rapidly to be accurately fit by a low-order polynomial. These two geocoronal lines fill the $2''$ slit, such that the lines are $\sim 50 \text{ \AA}$ wide in the gross counts spectrum, extending beyond the wavelength regions normally ignored by the polynomial fit. To accurately account for the background in the presence of these broad geocoronal lines, we turned off background smoothing in X1D, and subtracted the unsmoothed background spectrum at wavelengths shorter than 1350 \AA , while at longer wavelengths, we subtracted a fit to the background spectrum using a Legendre polynomial.

Although the geocoronal lines are subtracted as part of the background subtraction in the X1D software, the SNR in the net spectrum is roughly an order of magnitude lower than it is outside of the regions spanned by these lines. For a star that is well-centered in the slit, the geocoronal Lyman- α line will span $1190\text{--}1240 \text{ \AA}$ in the stellar spectrum, but for a star off-center, the Lyman- α line can span a region in the wavelength-corrected stellar spectrum that is offset by $\sim 25 \text{ \AA}$ in either direction, thus possibly including a potentially useful C III multiplet at 1176 \AA . For this reason, in our analysis below, the C abundance is generally derived from both this C III multiplet and C IV $\lambda\lambda 1548, 1551 \text{ \AA}$.

After finalizing the X1D extractions, the individual spectra for each star were combined with the IRAF SPLICE package. The combined spectra are shown in Figures 3 – 10. For most of the stars, 10 such individual spectra from a single slit position were combined to produce the final spectrum, but three stars (BHK2, BHK5, and U3) fall in the overlap between two slit positions (see Figure 1), and thus have 20 individual spectra and twice the nominal exposure time. Comparing the spectra obtained in the two distinct slit positions for these three stars shows good agreement, providing a check on

our extraction procedures. Besides the 24 hot stars with clean spectroscopy, a handful of other hot stars fell within the slit for each slit position, but we were unable to extract accurate spectra for these objects for a variety of reasons, such as overlapping spectra, spectra falling under the shadow of the detector repeller wire, spectra falling under a slit occulting bar, or spectra falling on detector artifacts.

3. MODELS

We interpret our far-UV spectra using synthetic spectra from several sources. For the unclassified object U3 and the relatively cool AGBM and BHB stars, we use the UVBLUE grid (Rodríguez-Merino et al. 2005). For the hot and nearly featureless spectra of U1 and U2, we compare to both simple blackbody models and the hottest stellar model of Rauch & Ringat (2011), which has $T_{\text{eff}} = 250,000$ K, $\log g = 7$, and mass fractions of 0.33, 0.5, 0.02, and 0.15 for He, C, N, and O, respectively. For the EHB and BHK stars that are the primary focus of this paper, we calculated non-LTE line-blanketed model atmospheres and synthetic spectra, using our TLUSTY (Hubeny & Lanz 1995) and SYNPEC programs⁸.

TLUSTY computes stellar model photospheres in a plane-parallel geometry, assuming radiative and hydrostatic equilibria. Departures from LTE are explicitly allowed for a large set of chemical species and arbitrarily complex model atoms, using our hybrid Complete Linearization/Accelerated Lambda Iteration method (Hubeny & Lanz 1995). More specifically, the model atmospheres allow for departures from LTE for 1132 levels and superlevels of 52 ions: H I, He I, He II, C I – C IV, N I – N V, O I – O VI, Ne I – Ne IV, Mg II, Al II, Al III, Si II – Si IV, P IV, P V, S II – S VI, Fe II – Fe VI. Details of the model atom setup are provided in Lanz & Hubeny (2003, 2007), and in Cunha et al. (2006) for updated Ne models.

The model grid spanned 17,500 K to 50,000 K in T_{eff} , with 2,500 K steps, and 4.75 to 6.25 in $\log g$, with 0.75 steps. For the chemical composition, we initially began with broad abundance categories. One grid was calculated at standard cluster abundances, with $[\text{Fe}/\text{H}] = -1.36$, $Y = 0.23$, and $[\alpha/\text{Fe}] = +0.3$. The other grids assumed enhanced Y values of 0.4, 0.7, and 0.99, with each value of Y accompanied by either normal C and N abundances or enhanced C and N abundances (up to 3% and 1% by mass, respectively; see Lanz et al. 2004). In order to match the absorption line equivalent widths and broader line-blanketing features in our BHK and EHB spectra, we generated new models at $Y = 0.23$ and $Y = 0.99$, with the abundances of C and Si varied individually, and the abundances of the Fe-peak elements varied together but independently from the elements outside of the Fe peak. In these models, we assumed $\log g = 5.5$, which should be representative of the surface gravities in the BHK and EHB stars, given the insignificant variations in the low-resolution far-UV spectral features over the full range of surface gravity in such stars.

After the detailed emergent UV spectrum for each model atmosphere was calculated with SYNPEC, they were shifted to the radial velocity of NGC 2808 (101.6 km s^{-1} ; Harris 1996). We then added the absorption from strong interstellar lines of H I ($1.9 \times 10^{21} \text{ cm}^{-2}$), C II ($6.8 \times 10^{18} \text{ cm}^{-2}$), C IV ($6.0 \times 10^{17} \text{ cm}^{-2}$), Si II ($1.7 \times 10^{17} \text{ cm}^{-2}$), Si IV ($7.6 \times 10^{16} \text{ cm}^{-2}$), O I ($6.0 \times 10^{18} \text{ cm}^{-2}$), and Al II ($5.0 \times 10^{16} \text{ cm}^{-2}$), using the observed spectra of U1 and U2 as a guide (Figure 3), given the lack of obvious photospheric features in these spectra (aside from He II). Our assumed H I column is nearly twice what one

would expect from the mean gas-to-dust ratio in the Galaxy (e.g., Bohlin et al. 1978), but there are significant variations in this ratio along any given sightline (e.g., Diplas & Savage 1994). It is also larger than the column of $1.2 \times 10^{21} \text{ cm}^{-2}$ found in the x-ray analysis of Servillat et al. (2008), but a column that low is strongly discrepant with the Lyman- α profile in our spectra. We then reddened the spectrum using the mean Galactic extinction curve of Fitzpatrick (1999), assuming $E(B-V) = 0.18 \text{ mag}$ (Brown et al. 2001, 2010).

4. ANALYSIS

4.1. Comparison of the Composite EHB and BHK Spectra

We begin our analysis with an empirical look at the composite spectra of both the EHB and the BHK samples. The stars in each sample span a similar range of $m_{\text{FUV}} - m_{\text{NUV}}$ color, but the BHK stars are $\sim 0.7 \text{ mag}$ fainter than the EHB stars (Figure 2). In Figure 11, we show the composite spectrum for all 7 of the normal EHB stars in our sample, compared to the composite spectrum for all 8 of the BHK stars (i.e., subluminescent EHB stars) in our sample. Several strong features are due almost exclusively to interstellar absorption, and are similar in both of the composite spectra: Si II $\lambda 1260 \text{ \AA}$, O I $\lambda 1301 \text{ \AA}$, Si II $\lambda 1304 \text{ \AA}$, C II $\lambda 1335 \text{ \AA}$, Si II $\lambda 1527 \text{ \AA}$, and Al II $\lambda 1670 \text{ \AA}$. At these temperatures, the Si IV $\lambda \lambda 1394, 1403 \text{ \AA}$ doublet has significant contributions from both photospheric and interstellar absorption, but the strength of this feature is similar in both composite spectra, implying that on average, there is not much difference in Si abundance between the two populations. The Lyman- α feature in these spectra is dominated by interstellar absorption, but the BHK composite spectrum clearly exhibits less Lyman- α absorption. Given the dominant contribution from interstellar absorption in this feature, the photospheric absorption must be much weaker in the BHK stars than in the EHB stars, in order to produce a noticeable difference in the combined interstellar and photospheric feature. The presence of weaker Lyman- α absorption in the BHK stars is consistent with both higher temperatures and/or a higher He abundance in the atmospheres of the BHK stars, which is what one would expect if the BHK stars are flash-mixed. Besides this difference in Lyman- α , there are strong distinctions between the BHK and EHB stars in four other absorption features: C III $\lambda 1176 \text{ \AA}$ (a multiplet of 6 lines), C III $\sim 1427 \text{ \AA}$ (from 15 lines spanning 1424–1429 \AA), C IV $\lambda \lambda 1548, 1551 \text{ \AA}$, and He II $\lambda 1640 \text{ \AA}$ (a triplet). The C III and He II features are purely photospheric, while the C IV feature includes both interstellar and photospheric contributions. The C and He features are clearly stronger in the composite BHK spectrum, as expected if the BHK stars are flash-mixed. These features become stronger at the higher abundances and higher temperatures expected in flash-mixed stars (Brown et al. 2001).

4.2. Individual EHB and BHK Spectra

We next turn to the individual spectra of the EHB and BHK stars in our sample. As stated earlier, our synthetic spectra were computed on a T_{eff} grid with 2,500 K spacing, initially employing broad abundance classes. For each star, we first selected a synthetic spectrum that reproduced the gross characteristics of the observed spectrum and photometry, and then altered the abundances of C, Si, and the Fe-peak elements to match the observed atmospheric features. At the resolution and SNR of our spectra, estimating the equivalent width

⁸ Available at <http://nova.astro.umd.edu>

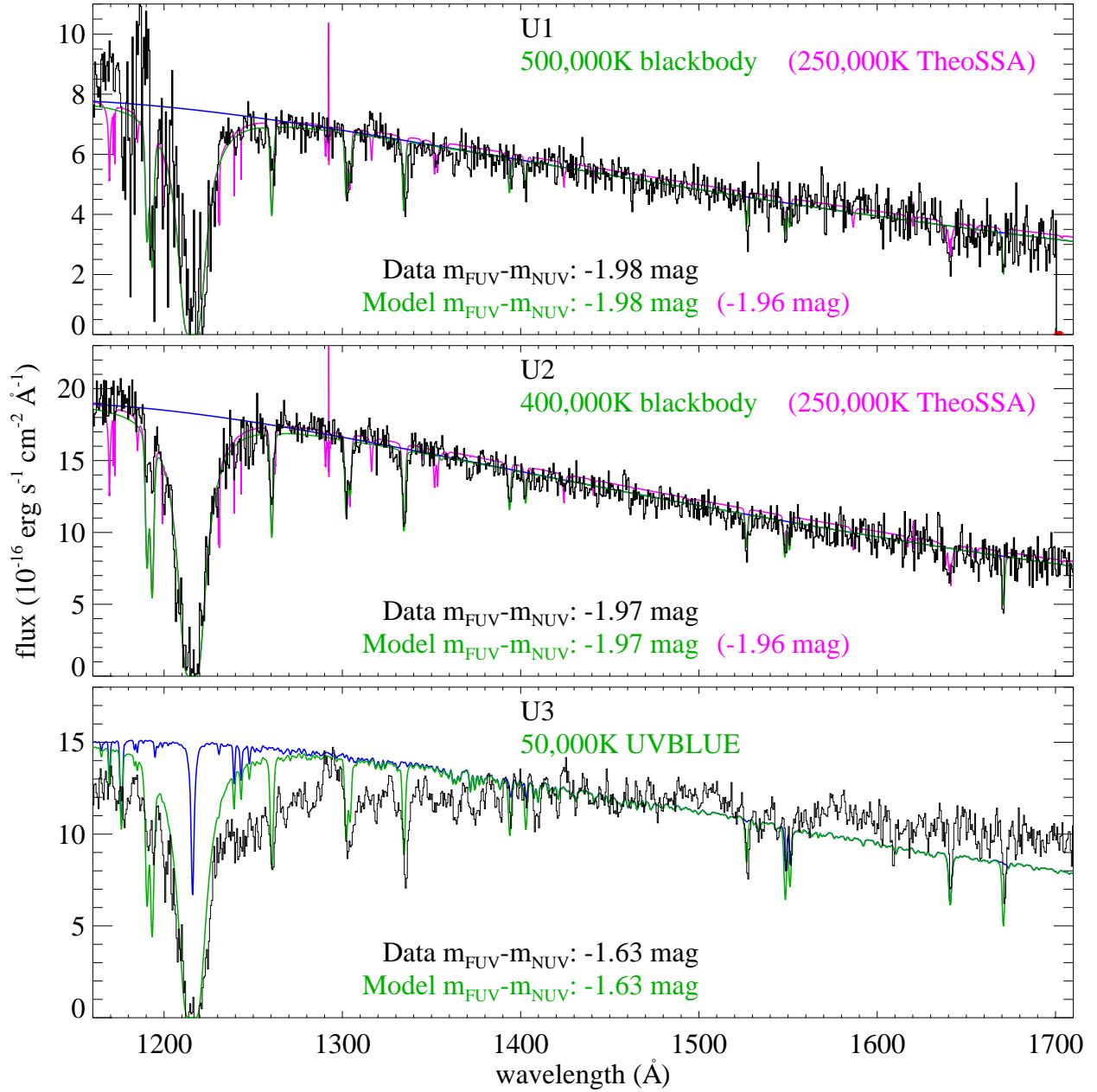


Figure 3. The spectra of our 3 unclassified objects (black histograms). In the top two panels, we compare the U1 and U2 spectra to blackbody models (without ISM absorption, blue; with ISM absorption, green) that approximately reproduce the far-UV spectral slope and the $m_{\text{FUV}} - m_{\text{NUV}}$ color, although the assumed temperatures are unphysically hot. We also compare these spectra to the hottest synthetic spectrum in the TheoSSA database (purple curves; Rauch & Ringat 2011). U1 and U2 are nearly featureless, other than interstellar absorption features and the He II absorption at 1640 Å. In the bottom panel, the UV photometry of U3 is consistent with a 50,000 K photosphere, but its UV spectrum looks much flatter than one would expect for this temperature. For comparison, we show the synthetic spectrum of a 50,000 K star at $[\text{Fe}/\text{H}] = -1.36$ (without ISM absorption, blue; with ISM absorption, green) interpolated from the UVBLUE grid (Rodríguez-Merino et al. 2005).

is hampered by the determination of the reference pseudo-continuum level in the presence of so many other lines. However, the data are of sufficient quality to characterize gross distinctions in abundance, at the level needed to detect the signature of flash mixing.

For simplicity, we will specify the abundances of C, Si, and the Fe-peak elements as multipliers on the abundances one would expect from a population at $[\text{Fe}/\text{H}] = -1.36$ with $[\alpha/\text{Fe}] = 0.3$. However, it is worth repeating that NGC 2808 hosts a triple main sequence (D’Antona et al. 2005; Piotto et al. 2007), with the reddest and bluest sequences exhibiting

clear chemical distinctions (Bragaglia et al. 2010). In particular, Bragaglia et al. (2010) found that a star on the blue MS in NGC 2808 had a lower C abundance ($[\text{C}/\text{Fe}] = -0.7$) than a star on the red MS ($[\text{C}/\text{Fe}] = -0.4$), as one would expect if the blue MS stars in NGC 2808 were formed from the He-rich ejecta of the first stellar generation. The C abundance in these MS stars would decrease even further due to the envelope mixing known to occur in globular cluster stars during the evolution up the RGB (Kraft 1994). Thus, one would expect the C abundance in the EHB stars of NGC 2808 to be strongly depleted, especially if they are the progeny of the blue MS

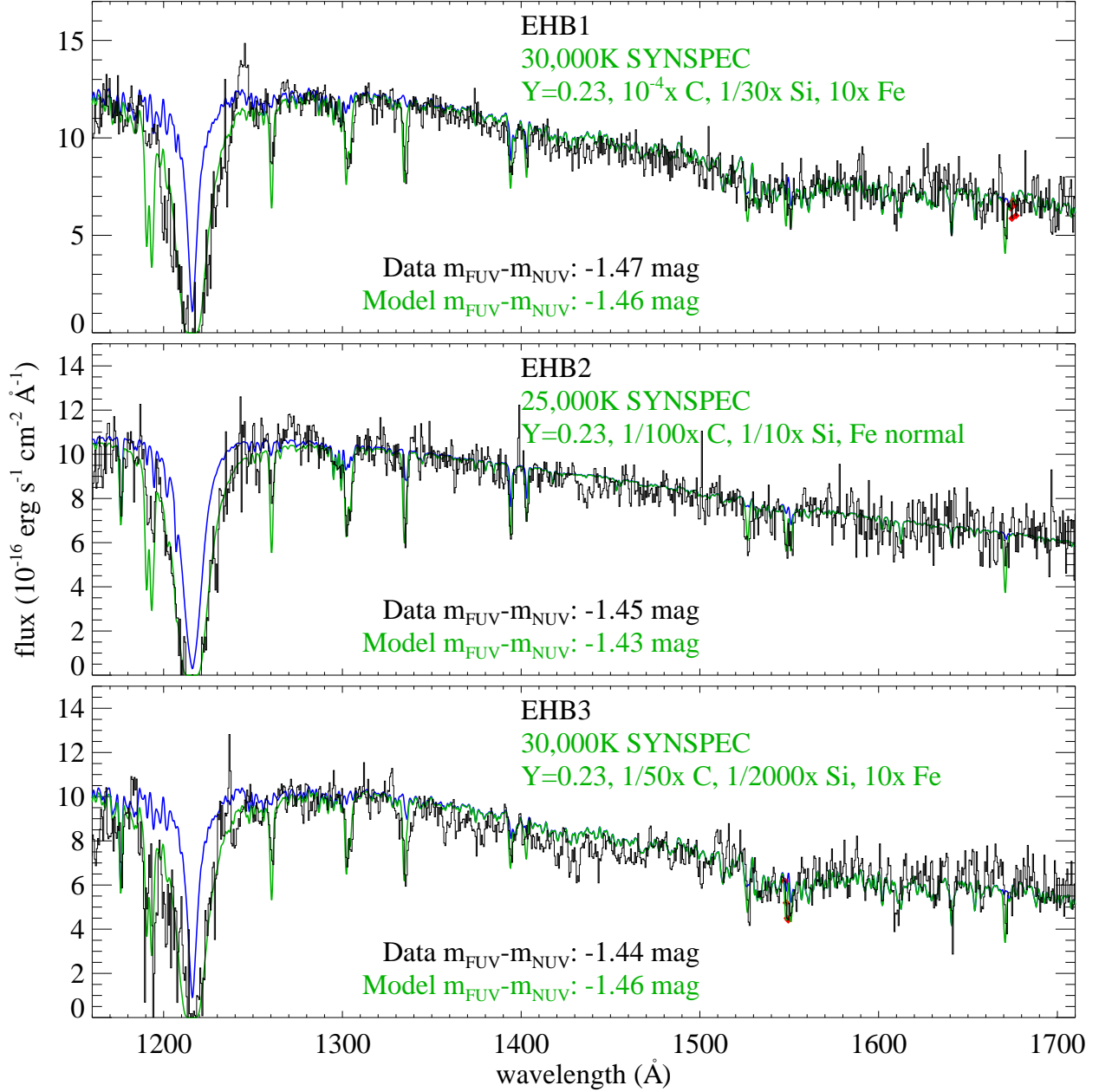


Figure 4. The spectra of three normal EHB stars (black histograms) compared to SYNSPEC synthetic spectra (without ISM absorption, blue; with ISM absorption, green) that approximately match the UV photometry and spectroscopy. The stars exhibit large abundance variations relative to the mean cluster abundance at the MS (labeled), presumably due to atmospheric diffusion. Data points with potential instrumental artifacts are flagged (red diamonds).

stars. In addition, atmospheric diffusion might decrease the C abundance in these EHB stars even further (Miller Bertolami et al. 2008).

Although the composite spectra of the BHk and EHB samples in Figure 11 show no obvious systematic difference in the Si abundance between the two classes, the Si abundance does show large star-to-star variations within each group (Figures 3–8). Most of the detectable Si features in our far-UV spectra are dominated by interstellar absorption, and none are completely photospheric, but Si IV $\lambda\lambda 1394, 1403$ Å does provide a rough indication of the stellar Si abundance. One star (EHB5; Figure 5) exhibits a Si abundance close to the cluster value, but most of the EHB and BHk stars exhibit weak to strong depletion of Si relative to the cluster value. For other stars (e.g., BHk5, BHk6, and BHk7; Figures 7 & 8), Si is de-

pleted by at least a factor of 1000. For photospheric Si abundances that are orders of magnitude below the cluster value, the Si IV feature is almost completely dominated by interstellar absorption, and the photospheric abundance we measure is an approximate upper limit. In general, our Si abundance is only accurate to an order of magnitude (see Figure 12).

With these spectra, there are no sufficiently isolated absorption lines from the Fe-peak elements that can be used to accurately characterize their abundances. However, the Fe-peak elements do cause broad absorption troughs in the far-UV spectrum that require large changes in the Fe-peak abundances in order to match the observed variations in the pseudo-continuum (Figure 13). The most obvious examples of this absorption can be seen in BHk7 and BHk8 (Figure 8), where the Fe-peak abundances are enhanced over the cluster

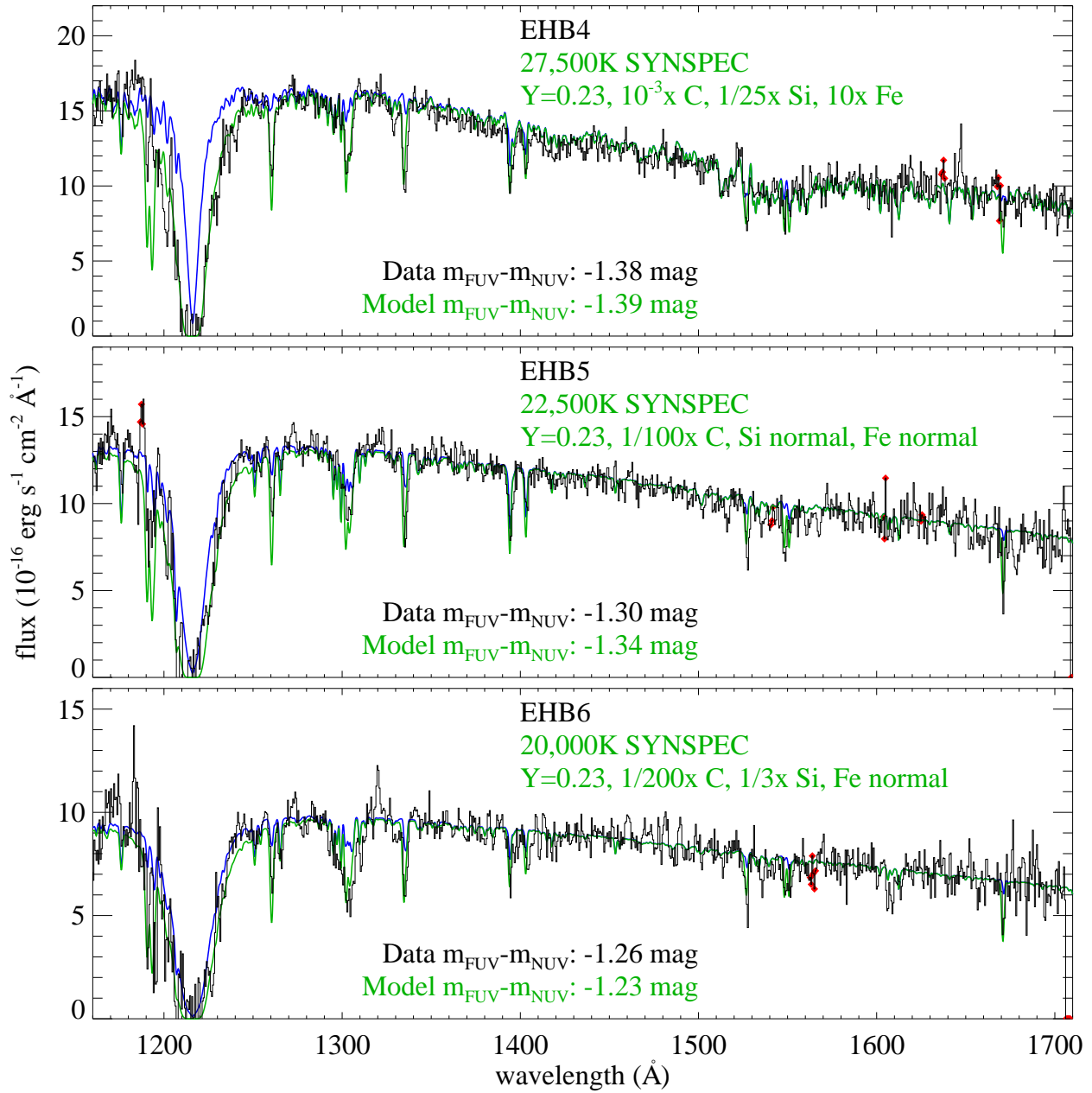


Figure 5. As in Figure 4, but for another three EHB stars with normal luminosities (black histograms) compared to SYNSEC synthetic spectra (without ISM absorption, blue; with ISM absorption, green).

value by factors of 25 and 100, respectively. Brown et al. (2001, 2010) have noted that some of the BHK stars in massive globular clusters are curiously red – much redder than one would expect from models for either normal EHB stars or BHK stars. BHK7 and BHK8 are in this group of curiously red BHK stars. Our spectra for these BHK stars show that their red colors can be explained by a large enhancement in their abundances of the Fe-peak elements. For comparison, models at the mean cluster abundance can match the $m_{FUV} - m_{NUV}$ colors of BHK7 and BHK8 only at much cooler temperatures of 16,900 K and 15,600 K, respectively; however, at such temperatures, the shape of the far-UV continuum in the synthetic spectra looks nothing like that observed. These large Fe-peak enhancements are required for the model to reproduce both the UV photometry and spectroscopy simultaneously. All of

the BHK stars show Fe-peak enhancements, ranging from $10\times$ to $100\times$ the cluster value, while the EHB stars are mixed, with three showing a $10\times$ enhancement and the other four showing no evidence for enhancement. Because the enhancement of Fe-peak elements does not come from the characterization of individual lines, the abundance uncertainty is approximately a factor of ~ 3 (Figure 13).

There are three clean C features in the far-UV spectra: the purely photospheric feature at 1176 Å from the C III multiplet, the purely interstellar feature at 1335 Å from the C II multiplet, and the C IV $\lambda\lambda 1548, 1551$ Å doublet that has both photospheric and interstellar contributions. There is also a photospheric feature at ~ 1427 Å arising from 15 C III lines (see Figure 11), but it is difficult to characterize in individual spectra, given its strength and blending with other features.

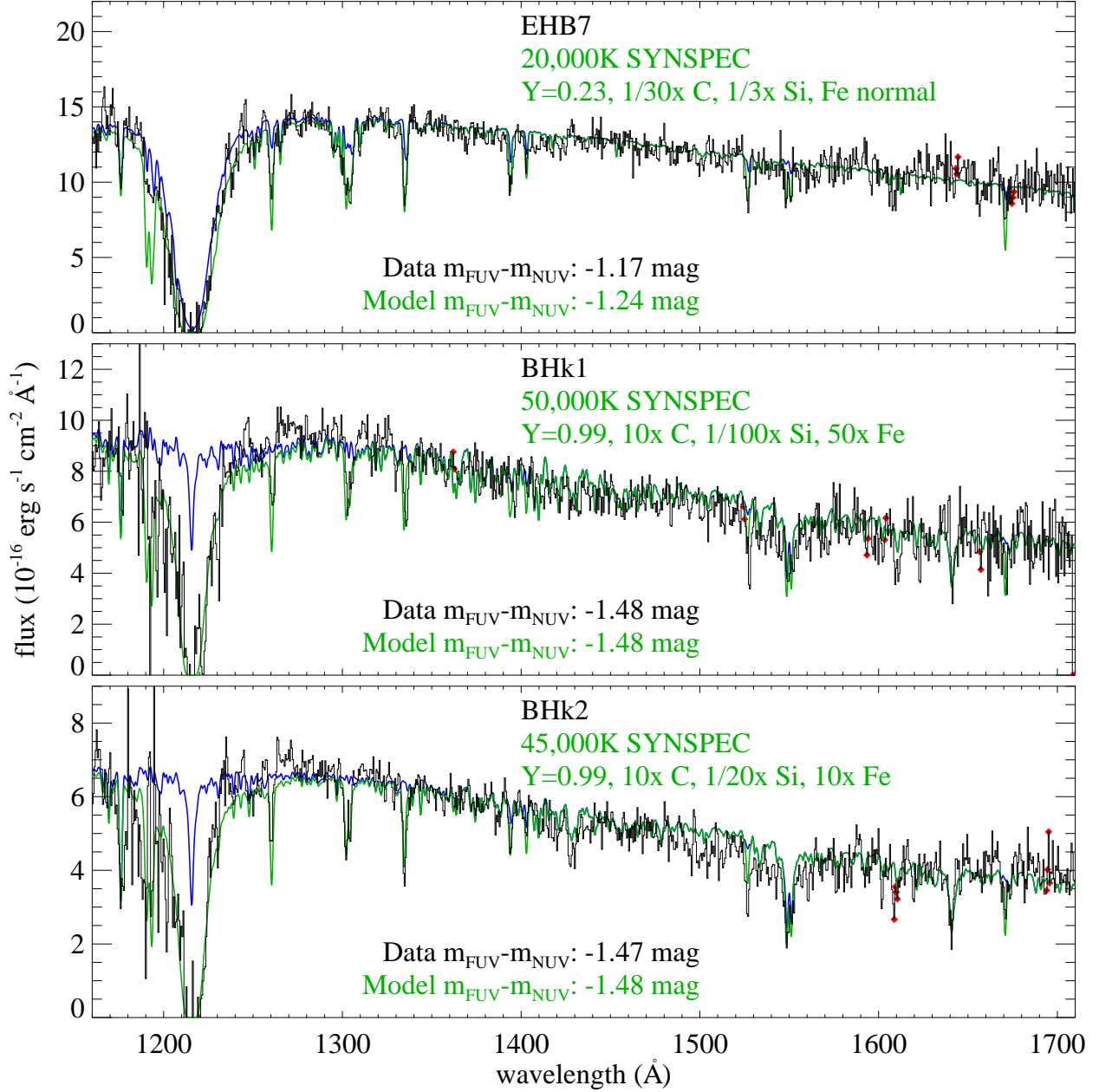


Figure 6. As in Figure 4, but for a normal EHB star and two BHk stars (black histograms) compared to SYNSPEC synthetic spectra (without ISM absorption, blue; with ISM absorption, green). The BHk stars exhibit much stronger He and C lines than the normal EHB stars.

Although the C III 1176 \AA feature potentially provides the best indicator of the stellar C abundance, in practice it frequently suffers from low SNR, relative to the C IV feature. This is because the C III 1176 \AA feature is affected to a varying degree by the Lyman- α geocoronal line (see §2). For this reason, we try to match the strength of both the C III 1176 \AA and C IV 1550 \AA features. In all of the EHB stars, the C abundance is depressed relative to that in the cluster, to varying degrees: C is depressed by a factor of 30 in EHB7, whereas C is nearly undetectable in EHB1, where it is depressed by a factor of 10,000. In the BHk sample, five of the stars (BHk1, BHk2, BHk4, BHk5, and BHk7) are enhanced in C (by factors of 3 to 10), two of the stars (BHk3 and BHk8) are somewhat depressed in C (by factors of 2 to 10), and one star (BHk6) is significantly depressed in C (by a factor of 400). Given the

SNR at C III and the interstellar contamination of C IV, our C abundances are generally accurate to a factor of ~ 2 (see Figure 12), but for those stars where the C abundance is orders of magnitude below the cluster value, our measured abundance is an approximate upper limit.

There is one significant He feature in the far-UV spectra: the purely photospheric He II feature at 1640 \AA . At the temperatures of EHB and BHk stars, the feature is mildly sensitive to abundance and very sensitive to T_{eff} . Furthermore, for these temperatures, the $m_{\text{FUV}} - m_{\text{NUV}}$ color does not significantly change if the He abundance is increased from $Y = 0.23$ to $Y = 0.4$, but it becomes ~ 0.1 – 0.3 mag redder if the He is increased to $Y = 0.99$. For this reason, the He abundance must be constrained by matching the far-UV spectral slope, the $m_{\text{FUV}} - m_{\text{NUV}}$ color, and the He II absorption feature si-

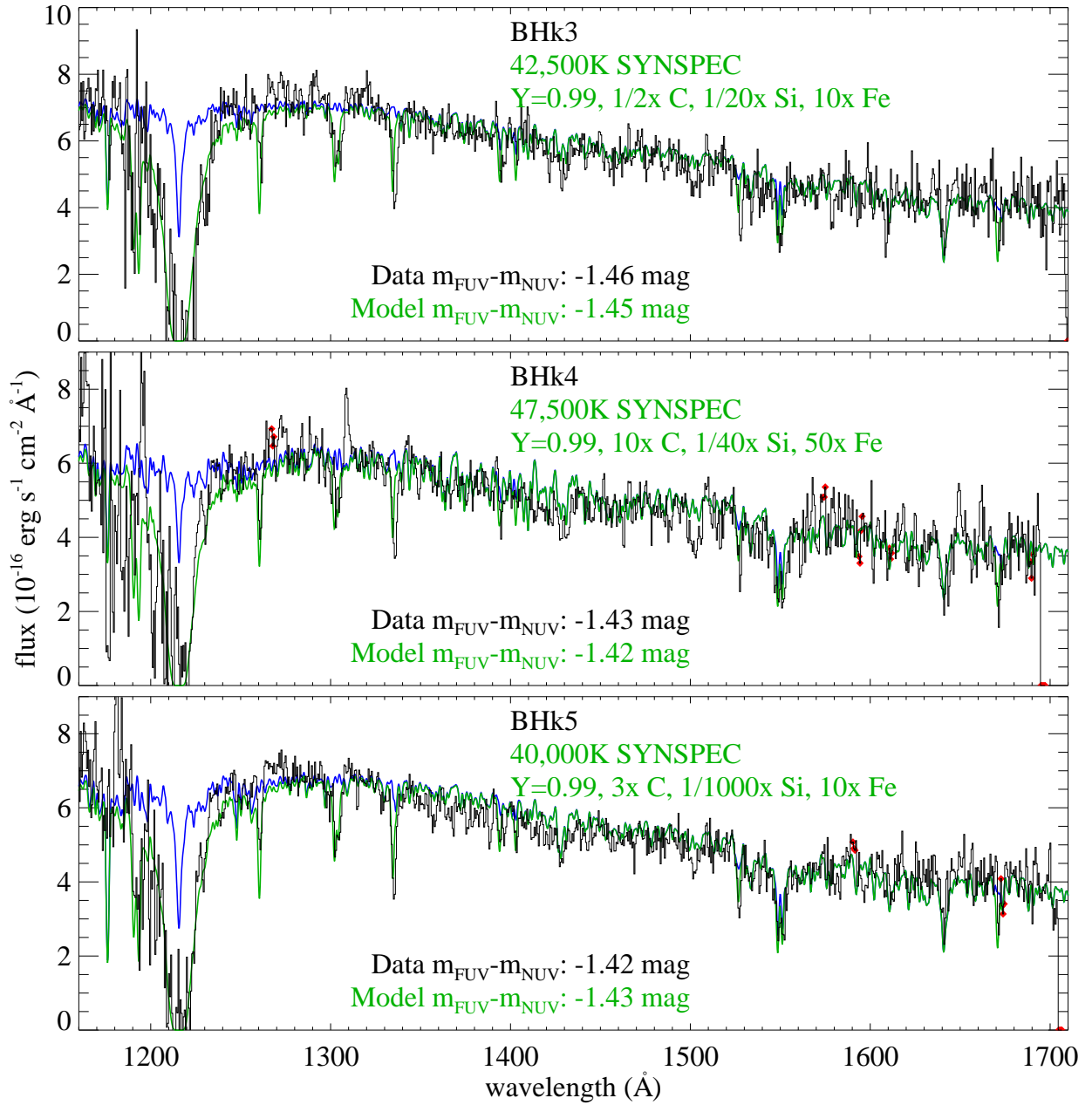


Figure 7. As in Figure 4, but for three more BHk stars (black histograms) compared to SYNPEC synthetic spectra (without ISM absorption, blue; with ISM absorption, green).

multaneously. In the EHB sample, these three aspects of each star can be approximated by a model at the standard cluster He abundance ($Y = 0.23$). The He II feature is difficult to characterize in the EHB sample, given the weakness of the feature at these cooler temperature, the relatively low SNR at the red end of the STIS spectrum, and the line blanketing in the vicinity of the feature; it is only obvious in the hottest stars of our EHB sample (EHB1 and EHB3). Although He is often depleted in EHB stars (e.g., see Moehler et al. 2011), reducing the He abundance from $Y = 0.23$ to $Y = 0.01$ has no significant effect on the far-UV spectral slope, while the $m_{FUV} - m_{NUV}$ color only changes at the ~ 0.01 mag level. That said, in those EHB stars where the feature is seen (EHB1 and EHB3), the equivalent width of He II is closer to that in a $Y = 0.23$ model than a $Y = 0.01$ model (Figure 14); for the remaining EHB

stars, the He abundance could be significantly depleted, and we would have no way of measuring it from the UV spectrum or photometry. In contrast, the He II feature is extremely strong in six of the BHk stars (BHk1, BHk2, BHk3, BHk4, BHk5, and BHk7), even though these stars have $m_{FUV} - m_{NUV}$ colors that are similar to those in the EHB sample. To simultaneously match the $m_{FUV} - m_{NUV}$ color and He II feature in each of these stars, the synthetic spectra must be much hotter than those used to match the EHB sample, with an atmosphere that is 99% He by mass (Figure 14).

To see why this is the case, we can compare stars in the EHB and BHk samples that have similar $m_{FUV} - m_{NUV}$ colors. For example, EHB1 (Figure 4) and BHk2 (Figure 6) have exactly the same $m_{FUV} - m_{NUV}$ color (-1.47 mag), they both exhibit enhanced abundances of the Fe peak elements

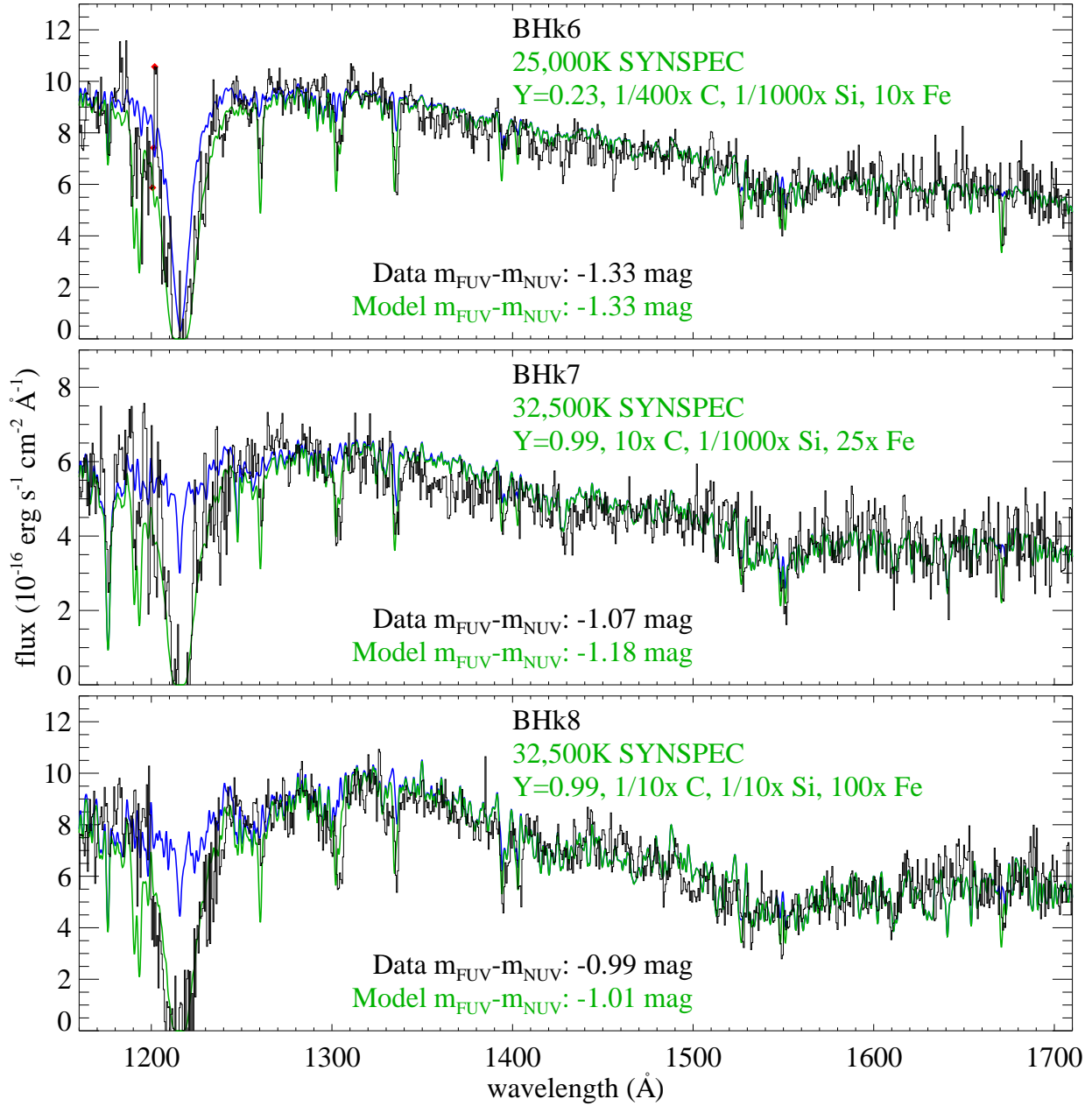


Figure 8. As in Figure 4, but for three more BHk stars (black histograms) compared to SYNSPEC synthetic spectra (without ISM absorption, blue; with ISM absorption, green). Unlike the other BHk stars in our spectroscopic sample, BHk6 shows no He and C enhancement, is relatively cool, and has a luminosity not much below the luminosity of the canonical EHB, so it is likely that the star did not undergo flash mixing. Compared to most of the BHk stars in our photometric sample, BHk7 and BHk8 have unusually red UV photometry, which may be explained by the strong enhancement of Fe, presumably due to atmospheric diffusion. Although the BHk8 spectrum does not exhibit a strong He II feature at 1640 Å, an enhanced He abundance in the model is needed to match both the UV photometry and far-UV spectroscopic continuum simultaneously (see text).

(10 times larger than the cluster mean), and they have similar Si abundances (20 to 30 times lower than the cluster mean). However, the BHk2 spectrum has much stronger C IV and He II lines than the spectrum of EHB1. The EHB1 spectrum is well-matched by a model at 30,000 K, but the BHk2 spectrum requires a model that is 15,000 K hotter. If one takes the BHk2 model shown in Figure 6 and reduces Y from 0.99 to 0.23 (while holding all other parameters fixed), the $m_{FUV} - m_{NUV}$ color increases to -1.60 mag, which is far bluer than the -1.47 ± 0.014 mag observed. Only a He-rich model reproduces the spectral slope, He II feature, and $m_{FUV} - m_{NUV}$ color. A similar argument can be made comparing EHB4

(Figure 5; $T_{\text{eff}}=27,000$ K, $m_{FUV} - m_{NUV}=-1.38$, $10\times$ enhanced Fe-peak elements, $25\times$ depleted Si) and BHk5 (Figure 7; $T_{\text{eff}}=40,000$ K, $m_{FUV} - m_{NUV}=-1.42$, $10\times$ enhanced Fe-peak elements, $1000\times$ depleted Si); EHB4 has very weak C IV absorption and no detectable He II absorption, while BHk5 has extremely strong C IV and He II absorption.

While most of the BHk sample exhibits obvious He enhancement, there are exceptions. The photometry and spectroscopy of BHk6 can be matched by a model that has a relatively low T_{eff} (25,000 K), depleted C abundance ($400\times$ lower than the cluster value), and $Y = 0.23$. The BHk8 spectrum does not appear to have a strong He II feature, but a $Y = 0.99$

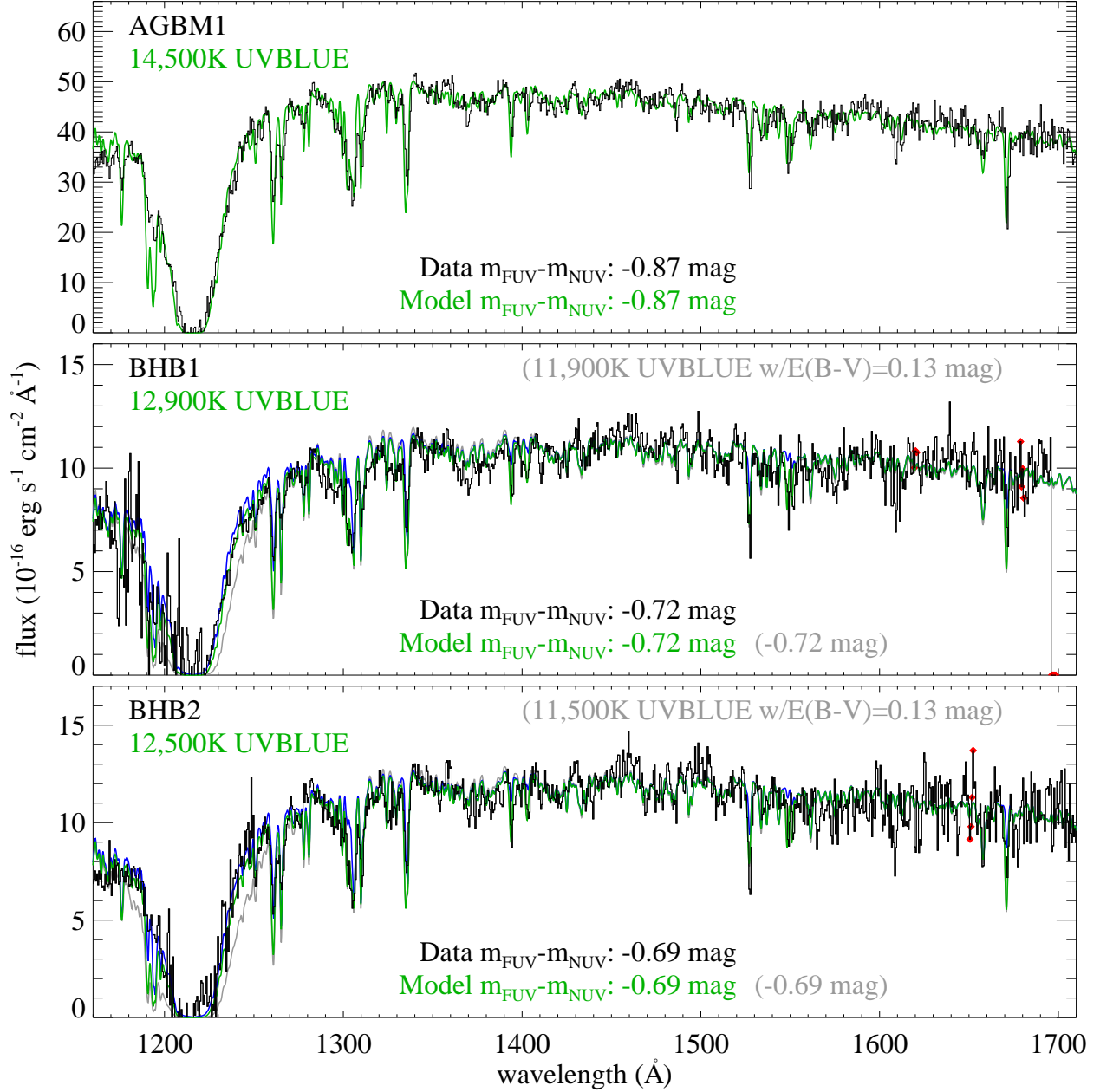


Figure 9. As in Figure 4, but for an AGBM star and two normal BHB stars (black histograms) compared to UVBLUE synthetic spectra (without ISM absorption, blue; with ISM absorption, green). The synthetic spectra were interpolated in temperature and metallicity from the UVBLUE grid to match the $m_{FUV} - m_{NUV}$ color at the cluster metallicity. For BHB1 and BHB2, we also show cooler models (grey) with less reddening, which can also reproduce the UV color but not simultaneously the Lyman- α profile. Thus, the temperature range of our BHB sample clearly includes the point (at $\sim 12,000$ K) where one expects to see a jump in Fe abundance, but in fact BHB1 and BHB2 do not exhibit significantly stronger line blanketing when compared to the cooler BHB stars in our sample (Figure 10).

model is required to simultaneously match the photometry and spectroscopic slope; reducing Y to 0.23, while holding the other parameters fixed, does not significantly impact the agreement with the far-UV spectrum, but makes the model $m_{FUV} - m_{NUV}$ color 0.3 mag bluer. Similar to BHK6, the BHK8 spectrum indicates a C abundance depleted with respect to the cluster value, although it is still much higher than that in the EHB sample.

To summarize, the EHB stars and BHK stars exhibit no systematic difference in Si abundance, but both classes exhibit large star-to-star variations in Si abundance, probably resulting from atmospheric diffusion. The Fe abundance also varies

strongly from star to star, but it is systematically higher in the BHK stars than in the EHB stars, and all of the BHK stars exhibit large Fe enhancements. The largest chemical distinctions between the EHB and BHK stars are those related to flash mixing (He and C). All of the EHB stars exhibit C abundances much lower than the cluster value, and He abundances at or below the solar value. As a group, the BHK stars are significantly hotter than the EHB stars, with five of them exhibiting enhanced C, and seven of them exhibiting enhanced He, which is strong evidence that most of the BHK population arises from flash mixing. The fact that He and C are not enhanced in the full BHK sample may indicate that some

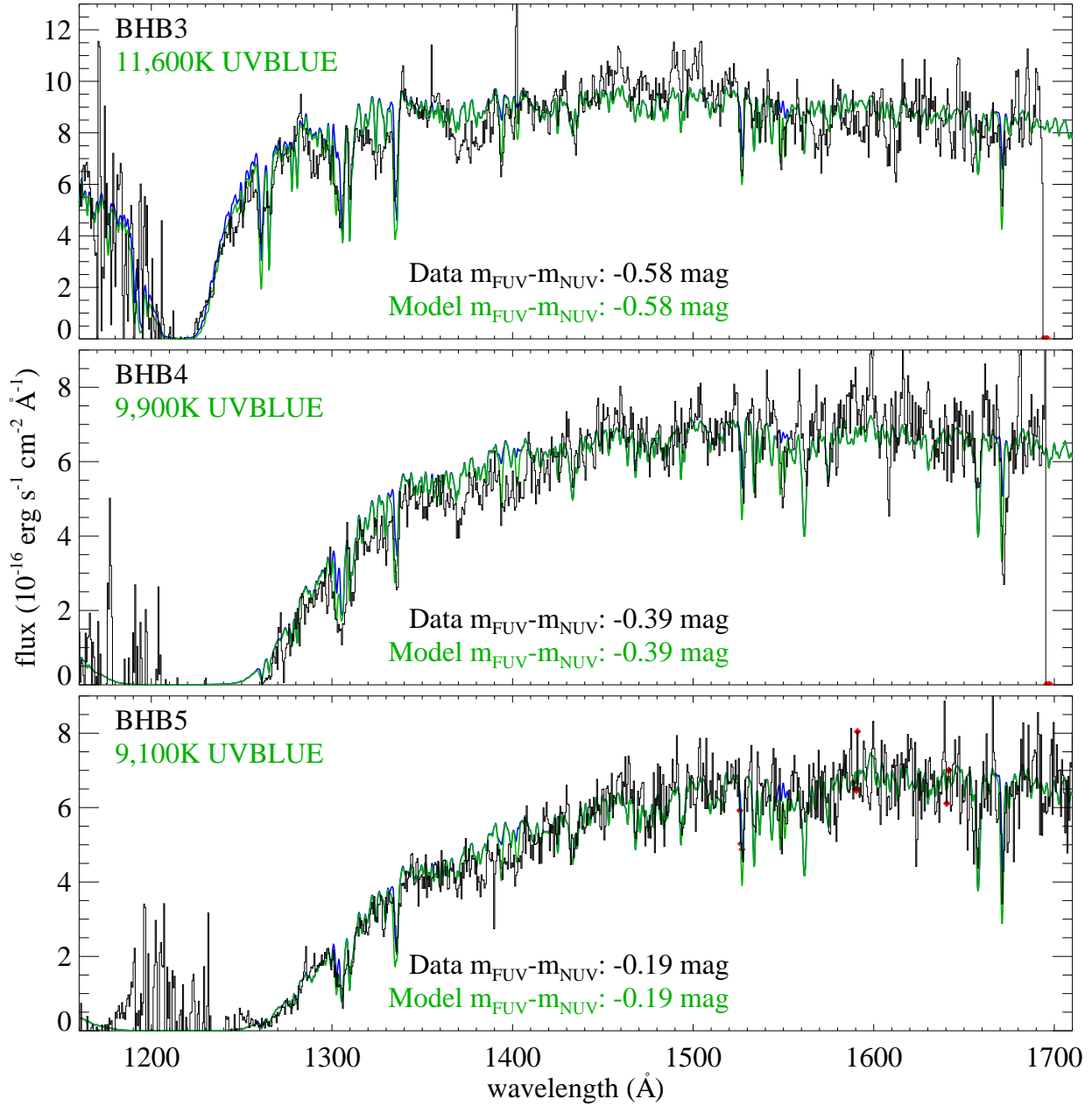


Figure 10. As in Figure 4, but for three more normal BHB stars (black histograms) compared to UVBLUE synthetic spectra (without ISM absorption, blue; with ISM absorption, green).

of these stars did not undergo flash mixing (e.g., BHK6), or that these elements were depleted due to atmospheric diffusion (e.g., BHK3 and BHK8; see Miller Bertolami et al. 2008).

4.3. Hot Unclassified Stars

Although the focus of this project is a comparison of the EHB and BHK samples in NGC 2808, our spectroscopic sample includes 9 other hot stars, which we briefly discuss here. Three of these stars (U1, U2, and U3) are hotter than the canonical HB (see Figure 2), and are labeled as unclassified. As with our BHK and normal EHB samples, the photometric uncertainties on these stars are small (see Figure 2), and there does not appear to be anything unusual about them in the UV images of the cluster (e.g., they do not appear to be blends, or to suffer from a detector artifact). Both U1 and U2 are hotter (bluer) than the evolutionary path a low-mass

star would take through the HR diagram as it begins to descend the white dwarf cooling curve, and they are also significantly brighter than the part of the white dwarf cooling curve where stars would begin to appear in any significant numbers, given the speed of the evolution between the HB and the white dwarf phases (e.g., see Figure 3 of Brown et al. 2001). The $m_{FUV} - m_{NUV}$ colors of U1 and U2 are implausibly blue compared to the expectations from evolutionary tracks for single stars, and the spectroscopy of these objects confirms that they are extremely hot (see Figure 3). U1 and U2 are consistent with blackbody temperatures of 400,000 K and 500,000 K, respectively, although both the UV photometric color and far-UV spectroscopic slope are becoming degenerate with temperature at such temperatures. More physically plausible would be the synthetic spectrum of a hot star. The

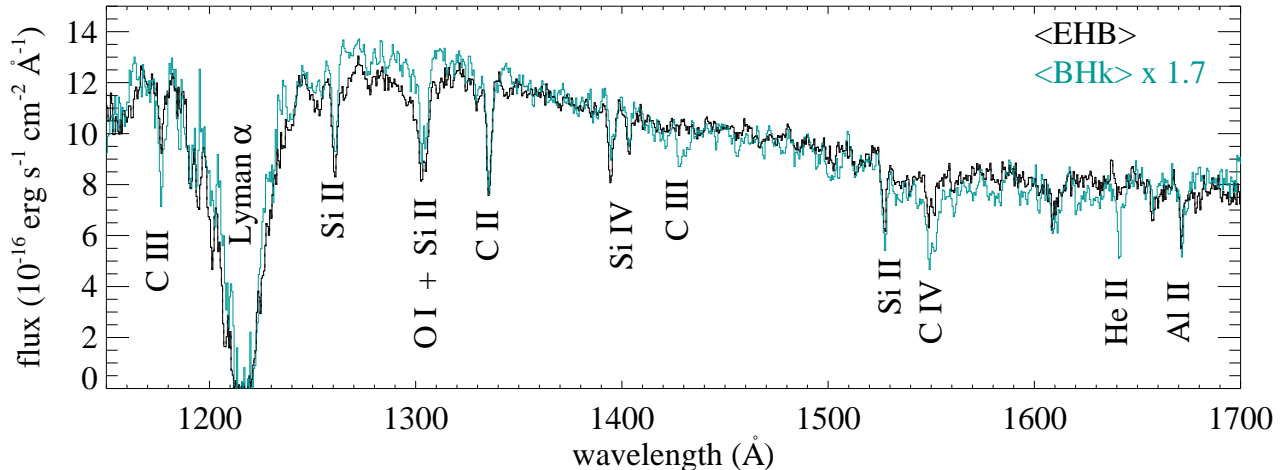


Figure 11. The composite spectrum for all EHB stars (black histogram) compared to that for all BHK stars (cyan histogram). The BHK spectrum has been multiplied by a factor of 1.7 in order to normalize the composite luminosity of the BHK stars to that of the EHB stars.

hottest model in the TheoSSA database of synthetic spectra for hot compact stars has a temperature of 250,000 K, and is in reasonable agreement with the UV spectral slope and photometry (Figure 3). However, if U1 and U2 have effective temperatures near 250,000 K, neither is actually compact; stars with that temperature and with the far-UV luminosities we observe would have radii similar to that of a low-mass post-AGB star that is about to descend the white dwarf cooling curve. The luminosities of U1 and U2 would be $\log L/L_{\odot} = 3.1$ and 3.5, respectively; such a high luminosity is at the extreme limit of that found for any globular cluster post-AGB star, and such temperatures are a factor of two higher than those found in low-mass post-AGB tracks. Note that some estimates for the foreground extinction toward NGC 2808 are higher than our value of $E(B-V) = 0.18$ mag. For example, Harris (1996) obtains $E(B-V) = 0.22$ mag from his assessment of the literature. Assuming a higher extinction would imply that even hotter intrinsic temperatures for U1 and U2 are needed to match the observed photometry and spectroscopy. Another possibility is that the extinction along the NGC 2808 sightline differs from the Galactic mean curve. Neither U1 or U2 appear to be coincident with x-ray sources in NGC 2808 (Servillat et al. 2008), but perhaps these objects are associated with accretion disks that could explain their unusually hot temperatures.

The unclassified star U3 is very puzzling. It has a very blue $m_{FUV} - m_{NUV}$ color in the NGC 2808 photometry, but its far-UV spectrum is much flatter than one would expect from a star with these UV colors. Perhaps the photometry and spectrum are the result of some kind of blend, non-stellar source, and/or circumstellar extinction, but we are unable to put forth a plausible explanation for the object. Like U1 and U2, U3 is not coincident with x-ray sources in NGC 2808 (Servillat et al. 2008). U2 and U3 respectively define the blue and red ends of a curious string of stars bluer than the canonical HB but all sharing approximately the same luminosity (see Figure 2).

4.4. BHB and AGBM Spectra

The AGBM and BHB stars in Figures 9 and 10 are well-matched by spectra from the UVBLUE (Rodríguez-Merino et al. 2005) grid, once these are interpolated to the NGC 2808 mean metallicity of $[\text{Fe}/\text{H}] = -1.36$ and to the effective temperatures that match the $m_{FUV} - m_{NUV}$ colors. The UVBLUE spectra do not provide the ability to independently vary in-

dividual elements, but the comparison between the synthetic spectra and data shows no gross signatures of atmospheric diffusion. The equivalent widths of the C and Si lines in our observed spectra are approximately matched by the lines in the synthetic spectra, although the C and Si lines are mostly dominated by interstellar absorption at these cooler temperatures. Furthermore, our AGBM and BHB spectra do not exhibit broad absorption troughs from the Fe-peak elements, indicating that the abundances of these elements are not greatly enhanced. This was unexpected, because our BHB sample brackets the temperature ($\sim 11,500$ K) where a discontinuity occurs in the Strömgren photometry of several globular clusters (Grundahl et al. 1999), which can be understood via sophisticated models of stellar evolution that self-consistently include the effects of atmospheric diffusion in the presence of turbulence (Michaud et al. 2008). In the globular cluster M13, which has a metallicity of $[\text{Fe}/\text{H}] = -1.5$ (i.e., only slightly lower than that of NGC 2808), the BHB stars hotter than this temperature exhibit an enhancement in the Fe abundance that approaches three times the solar abundance (Behr et al. 1999) – one to two orders of magnitude higher than cooler BHB stars and the mean cluster abundance. In NGC 2808 itself, Pace et al. (2006) found that BHB stars at or below 12,000 K exhibited no Fe enhancement, but that $[\text{Fe}/\text{H}]$ increases to ~ -0.7 at 12,200 K, ~ 0.1 at temperatures of 12,400–12,800 K, and then ~ 0.5 – 1.0 for stars hotter than 13,000 K. Assuming the same relationship between Fe enhancement and T_{eff} applies in our own sample, we would expect no enhancement in BHB3, BHB4, and BHB5, but enhancements of one to two orders of magnitude in BHB1 and BHB2. Such enhancements would be very obvious in the BHB1 and BHB2 spectra, but it is clear from Figures 9 and 10 that there is, in fact, little distinction in Fe abundance between BHB2 and BHB3 (the two stars bracketing the temperature of this transition).

Because we do not observe a jump in Fe abundance within the temperature range of our BHB sample, we explored the possibility that our temperatures are systematically too hot, but this does not seem likely. For example, by assuming a significantly lower extinction of $E(B-V) = 0.13$ mag, one could adopt temperatures for the BHB stars that are $\sim 1,000$ K cooler, thus placing them all below the temperature of 12,000 K where one expects a jump in the Fe abundance (see grey curves in Figure 9). However, the resulting far-UV synthetic spectrum has a Lyman- α profile much wider than

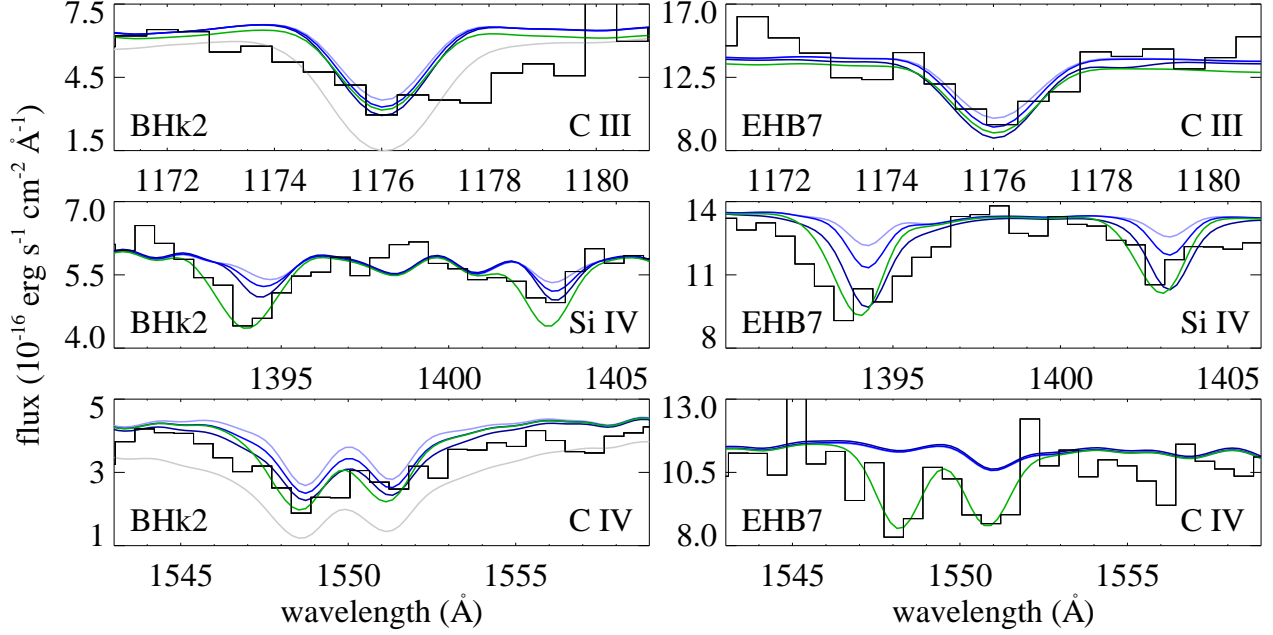


Figure 12. *Left panels:* The spectrum of BHK2 (black histogram), with the same model shown in Figure 6 (without ISM absorption, blue; with ISM absorption, green), in the vicinity of strong C and Si features. The resolution and SNR of the spectra in this program are sufficient to detect the gross abundance changes expected from flash mixing, but the uncertainties in our abundances are large. For comparison, we show two additional models (without ISM absorption): one with the Si reduced by a factor of 10 and the C reduced by a factor of 2 (lighter blue), and one with the Si increased by a factor of 10 and the C increased by a factor of 2 (darker blue). The C III feature (top panel) has almost no interstellar contribution, but the feature is not particularly sensitive to abundance in this regime, and this region of the spectrum is adversely affected by the proximity to the Lyman- α geocoronal line. The C IV feature (bottom panel) gives a good indication of the C abundance, but is complicated by the contribution from interstellar absorption, which can be significant for stars at low T_{eff} and low C abundance (see also Figures 3–10). The Si IV feature (middle panel) has a large contribution from interstellar absorption, and the photospheric component varies weakly with abundance. Although the C abundance in the BHK stars is strongly enhanced with respect to the normal EHB stars, it is not as strong as the 3% by mass one might expect for a star that has recently emerged from flash mixing. Despite the large uncertainties in the C abundance, a 3% C by mass can be firmly ruled out (grey). *Right panels:* The same features, but in the spectrum of EHB7, one of our coolest EHB stars. The model from Figure 6 is shown for comparison (without ISM absorption, blue; with ISM absorption, green), along with two additional models (without ISM absorption) that have C and Si reduced (lighter blue) and increased (darker blue) by factors of 2 and 10, respectively. For stars at low C abundance and the low end of the T_{eff} range in our sample (such as EHB7), the C IV feature is dominated by ISM absorption, and so the C abundance must be determined from the C III feature.

that observed, and the extinction would be much lower than most values adopted in the literature, including that of Pace et al. (2006), who assumed $E(B-V) = 0.22$ mag in their analysis. If one does not resort to a lower extinction, both the UV color and Lyman- α profile place tight constraints on the temperatures of the BHB stars. The statistical error in UV color is less than 0.02 mag for each star (see Figure 2), and so adopting a lower T_{eff} for each BHB star would require significant systematic errors in the STIS photometric calibration and also significant systematic errors in the Lyman- α profile of each model, both going in the same direction. In BHB1, adopting a T_{eff} of 12,200 K instead of 12,900 K at our nominal $E(B-V) = 0.18$ mag would incur a mismatch in UV color of 0.05 mag, with a gross mismatch in Lyman- α profile. Because the temperature leverage provided by the UV color improves at cooler temperatures, the constraints for the cooler BHB stars are even more stringent. Specifically, if one is willing to accept a 0.05 mag mismatch in UV color, BHB2 could be 600 K cooler, BHB3 could be 450 K cooler, BHB4 could be 200 K cooler, and BHB5 could be 150 K cooler. In each case, however, the Lyman- α profile of the cooler model would be much broader than observed.

The star AGBM1 is far brighter than the other stars in our sample, and its spectrum has the highest SNR. Although the observed spectrum is generally well-matched by the interpolated UVBLUE spectrum, there is a discrepancy in the strength of the interstellar Si II feature at 1190 Å (which arises from our interstellar absorption model, and not the UVBLUE grid). Although this feature falls within the region where the

SNR is depressed by the broad geocoronal Lyman- α line, the luminosity of this particular star means it still has adequate SNR to accurately measure this feature if present. In fact, the Si II $\lambda 1190$ Å feature is overpredicted by our interstellar absorption model for all of the stars in our entire sample, but our chosen Si II column does reproduce the other interstellar Si II features in the spectra.

5. DISCUSSION

Compared to the stars in our EHB sample, the stars in our BHK sample are significantly hotter, and have much higher He and C abundances. This can be seen from both an empirical comparison of the mean spectrum for each class, and also from a comparison of the models that best reproduce the individual stars in each class. NGC 2808 likely hosts a sub-population of MS stars born with an enhanced He abundance ($Y \sim 0.4$; D’Antona et al. 2005; Piotto et al. 2007), and such stars are more likely to produce EHB stars (including the EHB stars of normal luminosity and the subluminous BHK stars). However, the flash-mixing scenario is the only plausible mechanism for producing the higher temperatures and enhanced He and C abundances in our BHK sample.

Although the C abundance in our BHK sample is greatly enhanced relative to the EHB sample, it is not as high as one would expect for stars that underwent flash mixing very recently. The strongest enhancements of C in our BHK sample are at $10\times$ the cluster ratio of C to H, corresponding to a mass fraction of 0.2% in the atmosphere, whereas flash mixing is expected to produce stars with atmospheric C abundances of

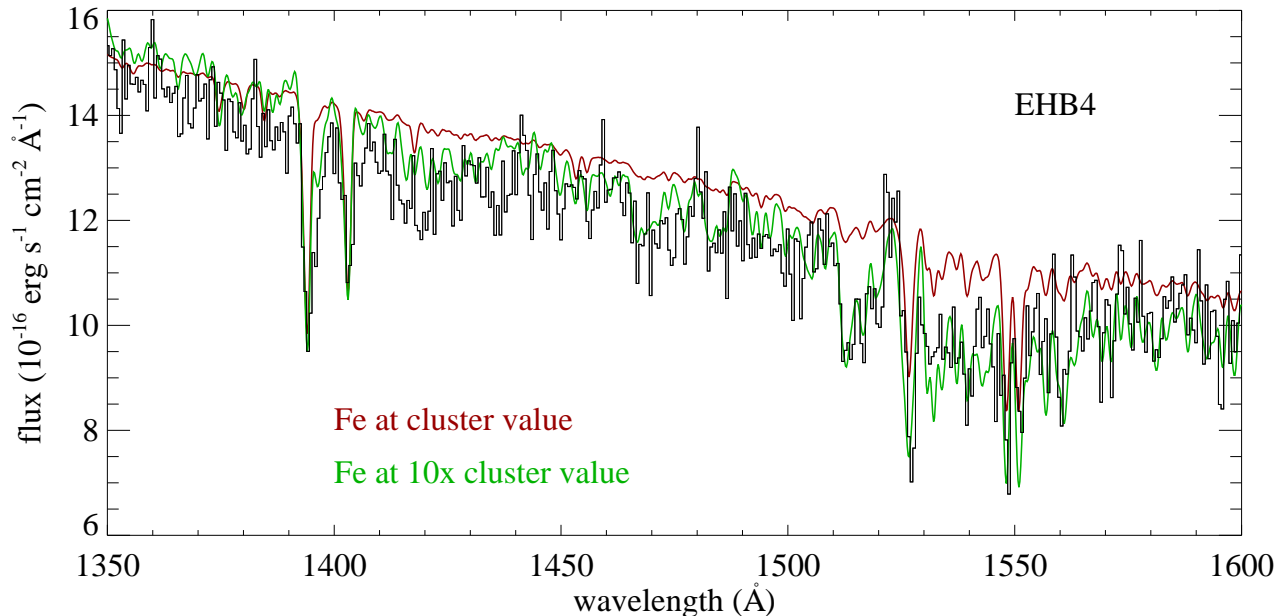


Figure 13. The spectrum of EHB4 (black histogram) in the vicinity of strong line-blanketing from the Fe-peak elements. For comparison, we show the best-fit model, where these elements are enhanced with respect to the cluster value by a factor of 10 (green; Figure 5), and a model where these elements have not been enhanced (dark red). We show an order-of-magnitude variation for clarity, given that the abundance estimate comes from a series of features over a broad wavelength range, but our uncertainty in the abundance of the Fe-peak elements is approximately a factor of 3.

1–4% by mass. The reduction in C abundance is not unexpected, however. Miller Bertolami et al. (2008) calculated numerical simulations of stars as they evolved through the flash-mixing stage and subsequent period of stable core He burning, taking into account the atmospheric diffusion processes of gravitational settling and radiative levitation. They found that stars emerge from the flash-mixing process with strongly enhanced He and C abundances, but that the C abundance declines rapidly, dropping by an order of magnitude after 1000 yr, and by several orders of magnitude by the time the star has evolved for some 10^7 yr after the flash mixing of the envelope. Thus, the star spends only a very small fraction of its stable core He-burning lifetime with a C abundance near its maximum of 1–4% by mass. Their calculations also show the He will eventually decline in the atmosphere as well, although this happens over a much longer timescale, such that the decline does not become significant until $\sim 10^6$ – 10^7 yr later. The fact that Lanz et al. (2004) found higher C abundances in two of the three He-sdB stars in their Galactic field sample may be a selection effect; in NGC 2808, the stars were selected by position in the UV CMD, but in the Galactic field, the stars were selected by He abundance. Even in globular clusters, there might be other systematic effects at play. In their optical spectroscopy of candidate BHK stars in ω Cen, Moehler et al. (2011) found significant enhancements of He and C in the hottest HB stars, but in their sample the C enhancement approached the 3% one would expect for stars that have recently undergone flash mixing. Whether this is due to systematic differences in approach (e.g., optical vs. UV spectroscopy) or intrinsic differences in the populations is unclear.

The variations in Si and Fe-peak abundances clearly demonstrate that atmospheric diffusion is significant in the EHB and BHK populations. Abundance anomalies have also been well-documented in the field population of sdB stars (e.g., Heber et al. 2000; O’Toole & Heber 2006; Blanchette et al. 2008; Heber 2009; Geier et al. 2010), where large enhancements in the Fe-peak elements (but not Fe itself) are ob-

served. However, recent calculations demonstrate that other processes, such as turbulent mixing and mass loss, may also play a role in these anomalies (Hu et al. 2011; Michaud et al. 2011). Our observations demonstrate that large enhancements in the Fe-peak elements can occur in the BHK stars, and may explain those BHK stars with unusually red UV colors (Brown et al. 2001, 2010). Two of the BHK stars in our spectroscopic sample were drawn from this unusually red segment of the BHK population in NGC 2808, and both exhibit enormous enhancements in the Fe-peak elements (25–100 \times the cluster value). Apparently a large dispersion in the abundances of Fe-peak elements, when combined with flash mixing, can provide the large color range observed in the BHK population of massive clusters.

The hottest BHK stars in our sample fall at temperatures similar to those of recently-discovered pulsating subdwarfs in ω Cen (Randall et al. 2011). The four pulsating subdwarfs in ω Cen are located near the BHK region of the ω Cen CMD, and Randall et al. (2011) derive $48,000 \text{ K} \lesssim T_{\text{eff}} \lesssim 52,000 \text{ K}$ from their optical spectroscopy. Randall et al. (2011) suggest that their sdO pulsators inhabit a newly-discovered instability strip; if that is the case, our hottest BHK stars (BHK1 & BHK4) may also be pulsators. The enhanced Fe-peak abundances observed in our hottest BHK stars may be significant, as radiative levitation appears to play a role in sdO pulsations (Fontaine et al. 2008). We note, however, that Randall et al. (2011) found subsolar He abundances for their pulsators, in contrast to the He-rich atmospheres found in our hottest BHK stars. One intriguing possibility is that the pulsators in ω Cen are evolved from BHK stars, which are known to exist in ω Cen; diffusion processes can convert a He-rich BHK star into a He-poor sdO (Miller Bertolami et al. 2008). If flash mixing is required to achieve these high EHB temperatures, then the dearth of analogous pulsators in the field population may be explained because flash mixing is more likely to occur in populations born at high He abundance ($Y \sim 0.4$), such as those subpopulations found in massive globular clusters.

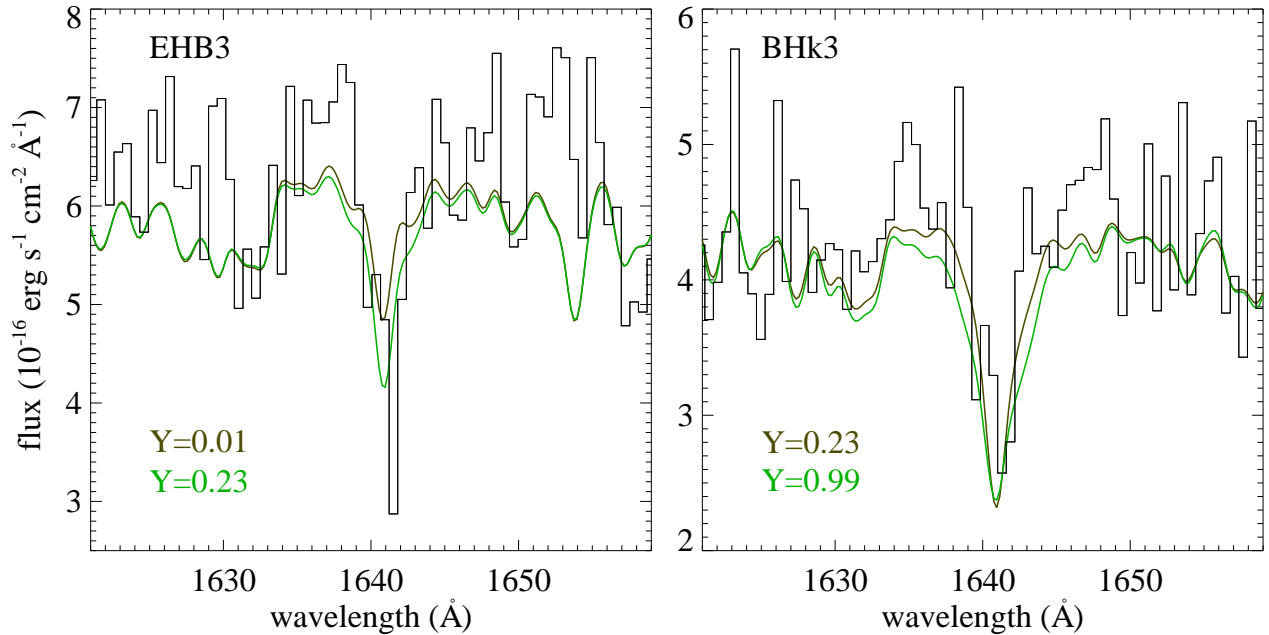


Figure 14. *Left panel:* The spectrum of EHB3 (black histogram), shown with the $Y = 0.23$ model of Figure 4 (green), compared to a model with all of the same parameters except for He abundance, which has been reduced to $Y = 0.01$ (brown). EHB stars are frequently depleted in He (e.g., Moehler et al. 2011), but in our sample, the spectra of EHB1 and EHB3 exhibit a detectable He II 1640 Å feature. The equivalent width of this feature in the data is better matched by the feature in the $Y = 0.23$ model than that in the $Y = 0.01$ model, although the feature is difficult to characterize when it is weak, given the line blanketing in this region and the relatively low SNR. Lowering the He from $Y = 0.23$ to $Y = 0.01$ has a negligible effect on the rest of the far-UV spectrum and the $m_{FUV} - m_{NUV}$ color; the $Y = 0.01$ model would be difficult to distinguish if shown in Figure 4. Aside from EHB1 and EHB3, the remaining EHB stars in our sample could be significantly depleted in He, but because they are significantly cooler, this feature is too weak to provide meaningful constraints on the He abundance. *Right panel:* The spectrum of BHk3, shown with the $Y = 0.99$ model of Figure 7 (green), compared to a model with all of the same parameters except for He abundance, which has been reduced to $Y = 0.23$ (brown). The He II 1640 Å feature is better-matched by the $Y = 0.99$ model (green), but, more importantly, the $Y = 0.23$ model has a much bluer $m_{FUV} - m_{NUV}$ color (-1.60 mag) than the $Y = 0.99$ model (-1.48 mag). If one reduces the T_{eff} in the $Y = 0.23$ model to try to match the $m_{FUV} - m_{NUV}$ color in the data (-1.47 mag), the He II feature in the model becomes even weaker, increasing the discrepancy with the feature observed in the spectrum. Moreover, the model does not match the observed far-UV spectral slope. Thus the simultaneous fitting of the He II feature, the $m_{FUV} - m_{NUV}$ color, and the far-UV spectral slope points to a high He abundance for BHk2.

Support for Program 11665 was provided by NASA through a grant from STScI, which is operated by AURA, Inc., under NASA contract NAS 5-26555. The TheoSSA service (<http://dc.g-vo.org/theossa>) used to retrieve a theoretical

spectrum for this paper was constructed as part of the activities of the German Astrophysical Virtual Observatory. We thank the anonymous referee for useful suggestions that improved the clarity of our manuscript.

REFERENCES

- Ahmad, A., & Jeffery, C.S. 2003, *A&A*, 402, 335
 Ahmad, A., Jeffery, C.S., & Fullerton, A.W. 2004, *A&A*, 418, 275
 Anderson, J. 1997, Ph.D. thesis, UCB
 Behr, B.B., Cohen, J.G., McCarthy, J.K., & Djorgovski, S.G. 1999, *ApJ*, 517, L135
 Blanchette, J.-P., Chayer, P., Wesemael, F., Fontaine, G., Fontaine, M., Dupuis, J., Kruk, J.W., & Green, E.M. 2008, *ApJ*, 678, 1329
 Bohlin, R.C., Savage, B.D., & Drake, J.F. 1978, *ApJ*, 224, 132
 Bragaglia, A., et al. 2010, *ApJ*, 720, L41
 Brown, T.M., Sweigart, A.V., Lanz, T., Smith, E., Landsman, W.B., & Hubeny, I. 2010, *ApJ*, 718, 1332.
 Brown, T.M., Ferguson, H.C., Davidsen, A.F., & Dorman, B.F. 1997, *ApJ*, 482, 685
 Brown, T.M., Smith, E., Ferguson, H.C., Sweigart, A.V., Kimble, R.A., & Bowers, C.W. 2008, *ApJ*, 682, 319
 Brown, T.M., Sweigart, A.V., Lanz, T., Landsman, W.B., & Hubeny, I. 2001, *ApJ*, 562, 368
 Busso, G., et al. 2007, *A&A*, 474, 105
 Cassisi, S., Schlattl, H., Salaris, M., & Weiss, A. 2003, *ApJ*, 582, L43
 Castellani, M., & Castellani, V. 1993, *ApJ*, 407, 649
 Cunha, K., Hubeny, I., & Lanz, T. 2006, *ApJ*, 647, L143
 Dalessandro, E., et al. 2011, *MNRAS*, 410, 694
 D’Antona, F., Bellazzini, M., Caloi, V., Pecci, F.F., Galletti, S., & Rood, R.T. 2005, *ApJ*, 631, 868
 D’Antona, F., Caloi, V., Montalbán, J., Ventura, P., & Gratton, R. 2002, *A&A*, 395, 69
 D’Cruz, N.L., Dorman, B., Rood, R.T., & O’Connell, R.W. 1996, *ApJ*, 466, 359
 D’Cruz, N.L., O’Connell, R.W., Rood, R.T., Whitney, J.H., Dorman, B., Landsman, W.B., Hill, R.S., Stecher, T.P., & Bohlin, R.C. 2000, *ApJ*, 530, 352
 Diplas, A., & Savage, B.D. 1994, *ApJS*, 93, 211
 Dotter, A., et al. 2010, *ApJ*, 708, 698
 Fitzpatrick, E.L. 1999, *PASP*, 111, 63
 Fontaine, G., Brassard, P., Green, E.M., Chayer, P., Charpinet, S., Andersen, M., & Portouw, J. 2008, *A&A*, 486, L39
 Fusi Pecci, F., & Bellazzini, M. 1997, in *The Third Conference on Faint Blue Stars*, ed. A.G.D. Phillip, J. Liebert, & R.A. Saffer (Schenectady: L. Davis Press), 255
 Geier, S., Heber, U., Edelmann, H., Morales-Rueda, L., & Napiwotzki, R. 2010, *Ap&SS*, 329, 127
 Gratton, R.G., Carretta, E., Bragaglia, A., Lucatello, S., & D’Orazi, V. 2010, *A&A*, 517, 81
 Grundahl, F., Catelan, M., Landsman, W.B., Stetson, P.B., & Anderson, M.I. 1999, *ApJ*, 524, 242
 Harris, W.E. 1996⁹, *AJ*, 112, 1487
 Heber, U., & Hirsch, H. 2010, *AIPC*, 1314, 79
 Heber, U. 2009, *ARAA*, 47, 211
 Heber, U., Reid, I.N., & Werner, K. 2000, *A&A*, 363, 198
 Hu, H., Tout, C.A., Glebbeek, E., & Dupret, M.-A. 2011, *MNRAS*, in press.
 Hubeny, I., & Lanz, T. 1995, *ApJ*, 439, 875
 Kraft, R.P. 1994, *PASP*, 106, 553
 Lanz, T., Brown, T.M., Sweigart, A.V., Hubeny, I., & Landsman, W.B. 2004, *ApJ*, 602, 342

⁹ 2010 Edition; Updated at <http://physwww.physics.mcmaster.ca/~harris/mwgc.dat>

- Lanz, T., & Hubeny, I. 2003, *ApJS*, 146, 417
Lanz, T., & Hubeny, I. 2007, *ApJS*, 169, 83
Michaud, G., Richer, J., & Richard, O. 2008, *ApJ*, 675, 1223
Michaud, G., Richer, J., & Richard, O. 2011, *A&A*, 529, 60
Miller Bertolami, M.M., Althaus, L.G., Unglaub, K., & Weiss, A. 2008, *A&A*, 491, 253.
Moehler, S., Dreizler, S., Lanz, T., Bono, G., Sweigart, A.V., Calamida, A., & Nonino, M. 2011, *A&A*, 526, A136
O'Toole, S.J.O., & Heber, U. 2006, *A&A*, 452, 579
Pace, G., Recio-Blanco, A., Piotto, G., & Momany, Y. 2006, *A&A*, 452, 493
Piotto, G., Bedin, L.R., Anderson, J., King, I.R., Cassisi, S., Milone, A.P., Villanova, S., Pietrinferni, A., & Renzini, A. 2007, *ApJ*, 661, L53
Piotto, G., et al. 2005, *ApJ*, 621, 777
Randall, S.K., Calamida, A., Fontaine, G., Bono, G., & Brassard, P. 2011, *ApJ*, 737, L27
Rauch, T., & Ringat, E. 2011, *ASPC*, 442, 563
Rich, R.M., et al. 1997, *ApJ*, 474, L25
Rodríguez-Merino, L.H., Chavez, M., Bertone, E., & Buzzoni, A. 2005, *ApJ*, 626, 411
Servillat, M., et al. 2008, *A&A*, 641, 654
Stroeer, A., Heber, U., Lisker, T., Napiwotzki, R., Dreizler, S., Christlieb, N., & Reimers, D. 2007, *A&A*, 462, 269
Sweigart, A.V. 1997, in *The Third Conference on Faint Blue Stars*, ed. A.G.D. Phillip, J. Liebert, & R.A. Saffer (Schenectady: L. Davis Press), 3